

# Simulation study on improving the spatial resolution of photon-counting hybrid pixel X-ray detectors

A. Krzyżanowska\* , R. Szczygieł 

AGH University of Science and Technology, 30 A. Mickiewicza Ave., 30-059 Krakow, Poland

## Article info

### Article history:

Received 10 Sep. 2021

Received in revised form 30 Oct. 2021

Accepted 2 Nov. 2021

Available online 15 Dec. 2021

### Keywords:

Charge-sharing, subpixel resolution, pixel detector, hit allocation, single photon counting.

## Abstract

Hybrid pixel radiation detectors with a direct photon-to-charge conversion working in a single photon counting mode have gained increasing attention due to their high dynamic range and noiseless imaging. Since sensors of different materials can be attached to readout electronics, they enable work with a wide range of photon energies. The charge-sharing effect observed in segmented devices, such as hybrid pixel detectors, is a phenomenon that deteriorates both spatial resolution and detection efficiency. Algorithms that allow the detection of a photon irrespective of the charge-sharing effect are proposed to overcome these limitations. However, the spatial resolution of the detector can be further improved beyond the resolution determined by the pixel size if information about the charge proportions collected by neighbouring pixels is used to approximate the interaction position. In the article, an approach to achieve a subpixel resolution in a hybrid pixel detector working in the single photon counting mode is described. Requirements and limitations of digital inter-pixel algorithms which can be implemented on-chip are studied. In the simulations, the factors influencing the detector resolution are evaluated, including size of a charge cloud, number of virtual pixel subdivisions, and detector parameters.

## 1. Introduction

Semiconductor pixelated sensors are widely used in spectroscopic and imaging applications. With the integration of analogue and digital structures and the scaling of CMOS technology, implementation of the complete signal processing path inside a pixel of size even down to tens of micrometres became possible [1]. In detectors with a direct photon-to-charge conversion, X-ray photons are absorbed and directly converted into electron-hole pairs. The operation principle of such detectors working in a single photon counting (SPC) mode is to create a pulse at a pixel electrode for each incoming photon. The signal, whose amplitude corresponds to the photon energy, is processed by an individual readout channel, and if it exceeds a threshold, it is counted by a pixel counter.

SPC detectors have an essentially infinite dynamic range and with their energy discrimination capabilities they provide noiseless imaging. Therefore, in spectral measurements, the photon energies can be distinguished with better resolution in comparison to integrating detectors [2]. The ability to work with multiple energy windows enables the imaging of multiple contrast media in medical X-ray imaging applications. Readout electronics projects for the SPC detectors of our research team are used, for example, in X-ray spectroscopy experiments of photon correlation [3,4], or dual-threshold imaging [5].

However, the performance of SPC detectors is limited by a pile-up. The answer to this problem is the optimization of the readout channel processing speed and the minimization of the pixel size which allows to minimize detector dead time and enables operation under the high flux conditions. However, when pixel sizes are very small, other phenomena, like charge-sharing, are responsible for a spatial resolution degradation. Registration of fractional

\*Corresponding author at: [krzyzanowska@agh.edu.pl](mailto:krzyzanowska@agh.edu.pl)

signals coming from one photon by several neighbouring pixels results in the signal amplitude being no longer proportional to the deposited energy. This leads to an increase of the false counts within lower energies in the spectrum. Simulations show that the charge-sharing effect in detectors of a pixel size of  $50 \times 50 \mu\text{m}^2$  causes severe distortions in the energy spectrum and spatial resolution [6].

Algorithms enabling detection of a photon irrespective of the charge-sharing effect were proposed to overcome these limitations [1]. The solutions implemented on-chip include the process of reconstructing charge and assigning a hit to a single pixel with the largest charge deposition [7–9] or, alternatively, the pattern recognition technique [10] and finding the centre of the charge cloud gravity [11].

However, the detector spatial resolution can be further improved beyond the resolution determined by the pixel size if information on the proportions of charge collected by neighbouring pixels is used to approximate the position of the photon-detector interaction. Therefore, the article is focused on the possible solutions that can be implemented on-chip which will improve the spatial resolution of the SPC detectors.

There are known off-chip solutions for integrating detectors [12,13] which solve the problems of distortions caused by charge-sharing. In this article, the authors focus on the on-chip approach to achieve a subpixel resolution in SPC detectors for soft X-ray applications. The aim of the study is to investigate the requirements of digital inter-pixel algorithms that can be implemented on-chip. The limitation of spatial resolution of SPC detectors with charge-sharing compensation techniques is achieved by the Medipix chip with a pixel pitch of  $55 \times 55 \mu\text{m}^2$  [7]. Therefore, the target spatial resolution of a new detector will be of  $50 \times 50 \mu\text{m}^2$  and below. It can be achieved by designing an algorithm reaching subpixel resolution implemented on-chip with a pixel pitch from 50 to 100  $\mu\text{m}$  and the final resolution will be the resulting product of the physical pixel size and the number of virtual pixel subdivisions. In the simulations, factors influencing detector resolution are evaluated, including charge cloud size, number of virtual pixel subdivisions, and detector parameters.

## 2. Materials and methods

The simulations performed have common assumptions derived from the previous experiments with a pixelated chip bonded to a sensor [8,14]. The charge spread between pixels was modelled with the Gaussian distribution. The detector parameters are presented in Table 1.

Table 1.  
The detector parameters used in the simulations.

Detector No.	Sensor material	Detector thickness ( $\mu\text{m}$ )	Bias voltage (V)	Photon energy (keV)	Noise ENC (e-rms)
1	Si	320	45	8	100
2	CdTe	1500	500	22	100

### 2.1. Analytical reconstruction of the hit position

The example of the charge cloud shared by nine pixels is presented in Fig. 1. If the charge in the pixels is integrated

over the X and Y axes, the resulting charges  $P_{XI}$ ,  $P_{XII}$ , and  $P_{XIII}$ , as well as  $P_{YI}$ ,  $P_{YII}$ , and  $P_{YIII}$  represent the cumulative charges seen by the columns and rows, respectively. Charges  $P_I$ ,  $P_{II}$ , and  $P_{III}$  collected by columns or rows are Gaussian distributed and can be expressed in the 1D case as a cumulative probability  $P(x \leq X)$  and calculated using an error function [15].

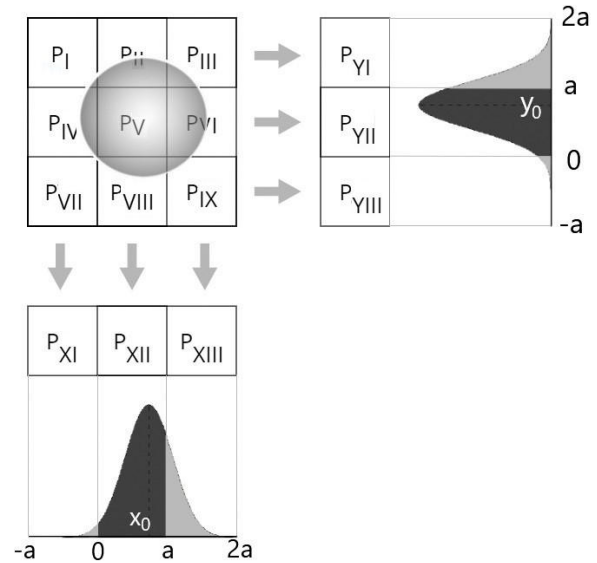


Fig. 1. View on the pixelated detector and charge cloud collected by the neighbouring nine pixels. The charge cloud integrated by rows and columns is used to extract the photon interaction position  $(x_0, y_0)$  based on the cumulative charge proportions.

The  $x_0$  represents the hit position and  $a$  represents the pixel size in the 1D case. Assuming the Gaussian distribution of the charge cloud,  $X$  is defined as the random variable describing the measurement position of the number of charge carriers. The  $X$  random variable is normally distributed with parameters:  $X \sim N(x_0, \sigma_x)$ , where  $x_0$  is the expected value of the hit position, and  $\sigma_x$  is the charge cloud sigma which is dependent on the detector parameters, such as thickness and bias voltage. Therefore, the estimated charge collected by the sensing unit in the interval  $(-\infty, x)$  can be expressed with the formula:

$$P(X \leq x) = \frac{1}{2} + \frac{1}{2} \operatorname{erf}\left(\frac{x - x_0}{\sigma_x \sqrt{2}}\right) \quad (1)$$

If pixels are considered sensing units and the charge cloud division between three pixels is assumed, the estimated charge ( $P_I$ ,  $P_{II}$ , and  $P_{III}$ ) collected by each of the three pixels can be described by the following equations:

$$P_I = P(X \leq 0) = \frac{1}{2} + \frac{1}{2} \operatorname{erf}\left(\frac{-x_0}{\sigma_x \sqrt{2}}\right) \quad (2)$$

$$P_{II} = 1 - P_I - P_{III} \quad (3)$$

$$P_{III} = 1 - P(X \leq a) = \frac{1}{2} + \frac{1}{2} \operatorname{erf}\left(\frac{x_0 - a}{\sigma_x \sqrt{2}}\right) \quad (4)$$

The  $x_a$  represents the hit position approximated by the algorithm. If the ideal algorithm is assumed and no

electronic noise is present,  $x_a = x_0$ . The simulation showed that assuming the given signal-to-noise ratio, the best result of estimation of the hit position was obtained when the approximated hit position was calculated based on the larger of two values  $P_I$  and  $P_{III}$ .

$$x_a = -\sigma_x \sqrt{2} \operatorname{erf}^{-1}(2P_I - 1) \quad (5)$$

$$x_a = \sigma_x \sqrt{2} \operatorname{erf}^{-1}(2P_{III} - 1) + a. \quad (6)$$

The 1D model can be generalized to the 2D model since the cumulative charge integrated by pixel columns and rows is normally distributed.

## 2.2. Reconstruction error

The reconstruction error  $\bar{e}$  was introduced to evaluate the allocation accuracy in the presence of noise. The measure of the distance between the actual hit position and the position of the reconstructed hit is given by Eq. (7):

$$\bar{e} = \frac{\sum_{n=0}^N \left( \frac{|x_0 - x_a| + |y_0 - y_a|}{2} \right)}{N}, \quad (7)$$

where  $(x_0, y_0)$  is the hit position,  $(x_a, y_a)$  is the reconstructed hit position, and  $N$  is the number of simulation steps.

The Monte Carlo method was used for all the simulations described in the article to calculate the reconstruction error  $\bar{e}$  for each interaction position in the presence of noise. The interaction position was changed within one pixel with a 1- $\mu\text{m}$  step. For each interaction position, the charge cloud was integrated over the neighbouring pixels, and, thus, the fractional charge collected by each pixel was calculated. For each interaction position, 1000 random ENC noise values with the Gaussian sigma distribution equal to 100  $\bar{e}$  were generated and added to the fractional signals in each pixel.

Finally, the interaction position was reconstructed and the mean reconstruction error was calculated.

## 2.3. Charge cloud parameters

The size of the charge cloud was determined by the detector parameters, such as the thickness  $d$ , the photon interaction depth  $\lambda$ , and the bias voltage  $V$ , according to Eq. (8) [16]:

$$\sigma_x = \sqrt{2kT(d - \lambda)^2 / qV}, \quad (8)$$

where  $k = 1.38 \cdot 10^{-23} \text{ J} \cdot \text{K}^{-1}$  is the Boltzmann constant,  $T = 300 \text{ K}$ , and  $q = 1.602 \cdot 10^{-19} \text{ C}$  is the unit charge.

If the detector thickness  $d \gg \lambda$ , the particle mean free path  $\lambda$  is negligible. However, for the Si sensor of the considered 8 keV photons and CdTe sensors recording 22 keV photons, the mean free paths  $\lambda$  calculated from the cross sections obtained from the NIST X-ray attenuation database [17] were of 67  $\mu\text{m}$  and 84  $\mu\text{m}$ , respectively. Since the sensors used in the previous investigation were 320- $\mu\text{m}$  thick in the case of Si and 1.5-mm thick in the CdTe case, the interaction depth was taken into account.

For the particular detector thickness, the desired  $\sigma_x$  can be achieved by applying a certain bias voltage. However,

the bias voltage value should be large enough to provide the detector full depletion.

## 3. Results

The three factors that influence the inter-pixel algorithm allocation error, namely the size of the charge cloud with respect to pixel size, number of the inside pixel subdivisions, and ADC resolution, were studied in the simulations.

### 3.1. The size of the charge cloud

The photon energy and detector material determine the number of charge carriers generated in a sensor volume which is also subject to fluctuations according to the Fano factor. Then, the carriers are collected by one or more pixels of the readout electronics, and the charge cloud spread depends on detector bias voltage, detector thickness, and photon interaction depth.

The aim of charge cloud modelling and charge cloud size simulations was to determine how many pixels should be involved in the reconstruction algorithm and to calculate the reconstruction precision that can be achieved assuming a certain noise level. The simulations were carried out to optimize the charge cloud sigma-to-pixel dimension ratio by minimization the reconstruction error. Assuming the Gaussian distribution of the charge induced in the detector and assuming that the charge is collected by a submatrix of  $3 \times 3$  pixels, the hit position was analytically derived from Eq. (5) and Eq. (6).

The simulation results show that, as presented in Fig. 2, the optimal ratio of the charge cloud size to the pixel size can be achieved for  $\frac{\sigma_x}{a} = 0.35$  with the reconstruction error reaching  $\bar{e} = 6.06 \mu\text{m}$ . The reconstruction error, as seen in Fig. 3, was the highest for the interactions occurring in the pixel centre because then the signals  $P_I$  and  $P_{III}$  had the lowest signal-to-noise ratio. It can be concluded that the final resolution improvement is a non-uniform function of the hit position. Moreover, the noise in each pixel registering fractional signals due to the charge spread should be low enough to allow setting the threshold low to work with low-energy photons.

The same simulations were performed for the charge spread in the area of  $5 \times 5$  pixels, leading to a three-fold increase of the reconstruction error. Therefore, this case was not further investigated.

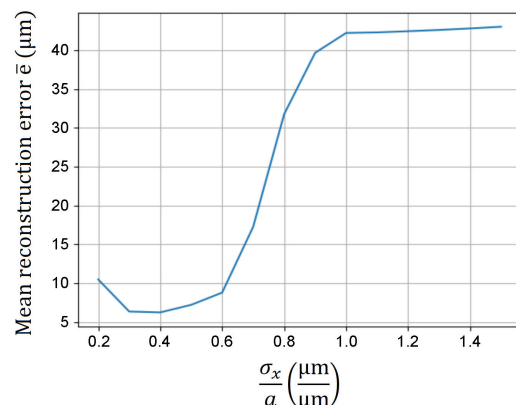
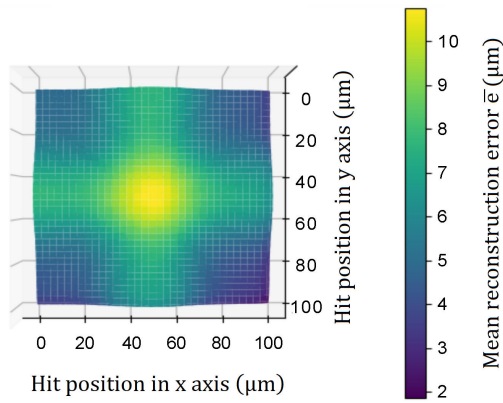


Fig. 2. The mean reconstruction error ( $\bar{e}$ ) as a function of the charge cloud sigma to the pixel size ratio.



**Fig. 3.** The reconstruction error for the optimal  $\sigma_x/a = 0.35$  as the function of the hit position.

If the  $\sigma_x/a$  is related to existing detectors, the bias voltage for the 320- $\mu\text{m}$  thick Si sensor should be lowered to the nominal full depletion voltage equal to  $V = 45\text{ V}$ . This gives  $\sigma_x = 8.57\text{ }\mu\text{m}$ . In the case of a 1500- $\mu\text{m}$  thick CdTe sensor, with a standard operation bias voltage,  $V = 500\text{ V}$ , and  $\sigma_x = 14.39\text{ }\mu\text{m}$ . The charge cloud parameters related to the pixel pitch of  $50 \times 50\text{ }\mu\text{m}^2$  and resulting reconstruction errors are presented in Table 2.

Table 2.

Results of the simulations for two detectors considered in Table 1 for the pixel pitch of  $50 \times 50\text{ }\mu\text{m}^2$ .

	Si detector $d = 320\text{ }\mu\text{m}$ $V = 45\text{ V}$	CdTe detector $d = 1500\text{ }\mu\text{m}$ $V = 500\text{ V}$
$\sigma_x$	8.57 $\mu\text{m}$	14.39 $\mu\text{m}$
$\sigma_x/a$	0.22	0.29
$\bar{e}$	8.99 $\mu\text{m}$	6.47 $\mu\text{m}$

### 3.2. Number of virtual subdivisions

The spatial resolution improvement can be achieved not only by scaling the pixel size, but also by minimizing the virtual subpixel size. The virtual subpixel is defined as a square unit within a physical pixel to which the hit is assigned. The greater the number of subpixels, the better allocation accuracy can be achieved. However, the number of subpixels that can be implemented is also limited by the silicon occupancy of the algorithm, since a counter must be placed in each subpixel.

The mean reconstruction error was calculated according to Eq. (7), taking  $(x_a, y_a)$  as the centre of the unit to which the hit was assigned. The simulation results presented in Fig. 4 show that the increase in the number of pixel subdivisions entailed a decrease in the mean reconstruction error. However, increasing the number of virtual units beyond  $5 \times 5$  resulted in a decrease in the mean reconstruction error by less than 5%.

The calculations were performed for the Si sensor and 8 keV photons. It should be considered that our detectors applications are soft X-ray experiments. However, the higher the energy beam, the better the signal-to-noise ratio. Thus, if the algorithm is designed for higher-energy photons, the reconstruction error can be decreased significantly by using clusters containing more pixels.

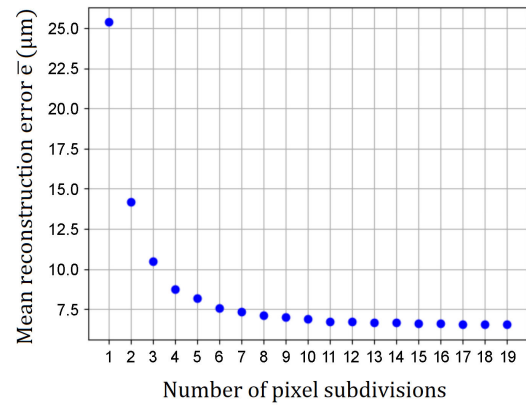


**Fig. 4.** The mean reconstruction error ( $\bar{e}$ ) as a function of the number of pixel subdivisions.

### 3.3. ADC resolution

A possible implementation of the inter-pixel algorithm involves placing an ADC in each readout channel which digitizes the voltage proportional to the charge collected by each pixel [15]. Then, digital logic based on the proportions of charge deposited in each pixel assigns the hit to the subpixel. Since the ADC resolution determines the silicon occupancy, the aim of the simulation was to study the impact of the ADC resolution on the mean reconstruction error.

The simulation results presented in Fig. 5 show a decrease in the mean reconstruction error with an increase in the number of ADC bits, reaching the value below  $10\text{ }\mu\text{m}$  for a 4-bit ADC. Furthermore, increasing the ADC resolution beyond 5 bits results in a decrease of the mean reconstruction error by less than 5%.

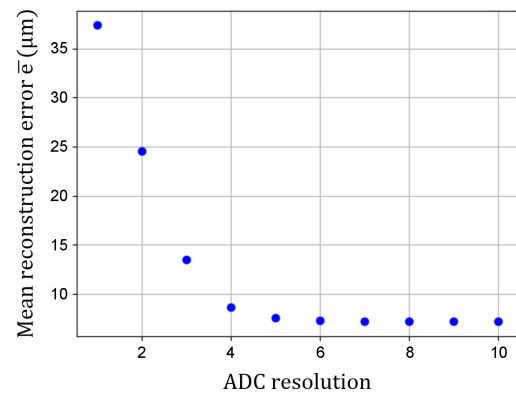


**Fig. 5.** The mean reconstruction error ( $\bar{e}$ ) as a function of the ADC resolution.

## 4. Conclusions

The influence of the optimal detection system parameters on the on-chip algorithm aiming to achieve the subpixel resolution of the hybrid pixel detector was studied. As a result, the requirements for the readout channel design and detector parameters were stated. The limits resulting from the simulation will serve as a guide for the inter-pixel algorithm design and implementation.

First, the inter-pixel algorithm should consider a pixel neighbourhood of  $3 \times 3$  pixels. Choosing a larger charge cloud size with respect to the pixel size did not improve the

reconstruction accuracy and implementing the algorithm that combines a larger neighbourhood of pixels requires more space inside each pixel. The minimum mean reconstruction error was achieved for the charge cloud size to a pixel size ratio given by  $\sigma_x/a = 0.35$ , which refers to the minimum reconstruction error  $\bar{\epsilon} = 6.06 \mu\text{m}$ . For a pixel pitch of  $50 \times 50 \mu\text{m}^2$ , if the Si sensor of  $320 \mu\text{m}$  is used, the standard operation bias voltage results in a reconstruction error above  $10 \mu\text{m}$ . The solution to reduce the error is to use the minimum bias voltage providing a full depletion, to reach the reconstruction error of  $\bar{\epsilon} = 8.99 \mu\text{m}$ . For a thicker  $1500\text{-}\mu\text{m}$  CdTe detector, the standard operation bias voltage provides the reconstruction error of  $\bar{\epsilon} = 6.47 \mu\text{m}$ . Therefore, a detector with a thicker CdTe sensor is a preferable solution.

Second, the number of virtual subpixels into which the pixel is divided should not be larger than  $5 \times 5$  assuming the ADC is used in the implementation of the inter-pixel algorithm. The 4-bit ADC resolution is sufficient to achieve the mean reconstruction error on a satisfactory level.

The target pixel pitch that provides the desired  $\sigma_x/a$  ratio is of  $50 \times 50 \mu\text{m}^2$ . The latest designs by our research group of readout circuits for X-ray SPC detectors show that the implementation of a 6-bit ADC designed in the 40-nm CMOS technology occupies an area of  $10 \times 30 \mu\text{m}^2$ . If a further scaling is needed, the design can be transmitted to newer technologies, e.g., 28 nm. A significant degree of inter-pixel connectivity will also be required, as it was already implemented in several previous projects [8,18]. Silicon occupancy of the inter-pixel algorithm blocks, which is dependent on the chosen technology node, will impose additional restrictions on the algorithm design.

To conclude, the presented simulations show that the reconstruction error of the ideal subpixel resolution algorithm can be maintained below  $10 \mu\text{m}$  for a  $1500\text{-}\mu\text{m}$  thick CdTe sensor (with standard bias setting) or for a  $320\text{-}\mu\text{m}$  thick Si sensor (with full depletion bias setting), with a 4-bit ADC implemented in the readout channel and  $4 \times 4$ -pixel subdivisions.

### Authors' statement

Research concept and design, A. Krzyżanowska and R. Szczygieł; collection and/or assembly of data, A. Krzyżanowska; data analysis and interpretation, A. Krzyżanowska and R. Szczygieł; writing the article, A. Krzyżanowska and R. Szczygieł; critical revision of the article, A. Krzyżanowska; final approval of article, A. Krzyżanowska.

### Acknowledgements

This research was funded by the National Science Centre, Poland, under Contract No. UMO-2018/29/N/ST7/02770. Author would like to thank the Polish Ministry of Education and Science for financial support in 2021.

### References

- [1] Ballabriga, R. et al. Review of hybrid pixel detector readout ASICs for spectroscopic X-ray imaging. *J. Instrum.* **11**, P01007–P01007 (2016). <https://doi.org/10.1088/1748-0221/11/01/P01007>
- [2] Taguchi, K. & Iwaczyk, J. S. Vision 20/20: Single photon counting X-ray detectors in medical imaging. *Med. Phys.* **40**, 100901 (2013). <https://doi.org/10.1118/1.4820371>
- [3] Bahadur, D. et al. Evolution of structure and dynamics of thermo-reversible nanoparticle gels—A combined XPCS and rheology study. *J. Chem. Phys.* **151**, 10 (2019). <https://doi.org/10.1063/1.5111521>
- [4] Sheyfer, D. et al. Nanoscale critical phenomena in a complex fluid studied by X-ray photon correlation spectroscopy. *Phys. Rev. Lett.* **125**, 125504 (2020). <https://doi.org/10.1103/PhysRevLett.125.125504>
- [5] Szczygieł, R., Grybos, P., Maj, P. & Zoladz, M. PXD18k - Fast Single Photon Counting Chip with Energy Window for Hybrid Pixel Detector. in 2011 IEEE Nuclear Science Symposium Conference Record. 932–937 (IEEE, Valencia, Spain 2011). <https://doi.org/10.1109/NSSMIC.2011.6154126>
- [6] Nilsson, H. E., Dubari, E., Hjelm, M. & Bertilsson, K. Simulation of photon and charge transport in x-ray imaging semiconductor sensors. *Nucl. Instrum. Methods Phys. Res. A* **487**, 151–162 (2002). [https://doi.org/10.1016/S0168-9002\(02\)00959-2](https://doi.org/10.1016/S0168-9002(02)00959-2)
- [7] Ballabriga, R. et al. The Medipix3RX: a high resolution, zero dead-time pixel detector readout chip allowing spectroscopic imaging. *J. Instrum.* **8**, C02016–C02016 (2013). <https://doi.org/10.1088/1748-0221/8/02/C02016>
- [8] Krzyżanowska, A. et al. Characterization of the photon counting CHASE Jr., chip built in a 40-nm CMOS process with a charge-sharing correction algorithm using a collimated X-ray beam. *IEEE Trans. Nucl. Sci.* **64**, 2561–2568 (2017). <https://doi.org/10.1109/TNS.2017.2734821>
- [9] Bellazzini, R. et al. PIXIE III: a very large area photon-counting CMOS pixel ASIC for sharp X-ray spectral imaging. *J. Instrum.* **10**, C01032–C01032 (2015). <https://doi.org/10.1088/1748-0221/10/01/C01032>
- [10] Otfinowski, P. et al. Comparison of allocation algorithms for unambiguous registration of hits in presence of charge-sharing in pixel detectors. *J. Instrum.* **12**, C01027–C01027 (2017). <https://doi.org/10.1088/1748-0221/12/01/C01027>
- [11] Otfinowski, P., Deptuch, G.W. & Maj, P. Asynchronous approximation of a center of gravity for pixel detectors' readout circuits. *IEEE J. Solid-State Circuits* **53**, 1550–1558 (2018). <https://doi.org/10.1109/JSSC.2018.2793530>
- [12] Cartier, C. et al. Micron resolution of MÖNCH and GOTTHARD, small pitch charge integrating detectors with single photon sensitivity. *J. Instrum.* **9**, C05027–C05027 (2014). <https://doi.org/10.1088/1748-0221/9/05/C05027>
- [13] Dreier, E. S. et al. Virtual subpixel approach for single-mask phase-contrast imaging using Timepix3. *J. Instrum.* **14**, C01011 (2019). <https://doi.org/10.1088/1748-0221/14/01/C01011>
- [14] Maj, P. et al. Measurements of ultra-fast single photon counting chip with energy window and  $75 \mu\text{m}$  pixel pitch with Si and CdTe detectors. *J. Instrum.* **12**, C03064 (2017). <https://doi.org/10.1088/1748-0221/12/03/C03064>
- [15] Krzyżanowska, A., Niedzielska, A. & Szczygieł, R. Charge-sharing simulations for new digital algorithms achieving subpixel resolution in hybrid pixel detectors. *J. Instrum.* **15**, C02047 (2020). <https://doi.org/10.1088/1748-0221/15/02/C02047>
- [16] Lutz, G. *Semiconductor Radiation Detectors, Device Physics*. (Berlin, Heidelberg: Springer Berlin Heidelberg, 2007).
- [17] NIST XCOM: Photon Cross Sections Database – Introduction. *NIST* <http://www.physics.nist.gov/PhysRefData/Xcom/Text/intro.html> (2017).
- [18] P. Otfinowski, A. et al. Pattern recognition algorithm for charge-sharing compensation in single photon counting pixel detectors. *J. Instrum.* **14**, C01017 (2019). <https://doi.org/10.1088/1748-0221/14/01/C01017>